Biological Chemistry ‘Just Accepted’ Papers

Biological Chemistry ‘Just Accepted’ Papers are papers published online, in advance of appearing in the print journal. They have been peer-reviewed, accepted and are online published in manuscript form, but have not been copy edited, typeset, or proofread. Copy editing may lead to small differences between the Just Accepted version and the final version. There may also be differences in the quality of the graphics. When papers do appear in print, they will be removed from this feature and grouped with other papers in an issue.

Biol Chem ‘Just Accepted’ Papers are citable; the online publication date is indicated on the Table of Contents page, and the article’s Digital Object Identifier (DOI), a unique identifier for intellectual property in the digital environment (e.g., 10.1515/hsz-2011-xxxx), is shown at the top margin of the title page. Once an article is published as **Biol Chem ‘Just Accepted’ Paper** (and before it is published in its final form), it should be cited in other articles by indicating author list, title and DOI.

After a paper is published in **Biol Chem ‘Just Accepted’ Paper** form, it proceeds through the normal production process, which includes copy editing, typesetting and proofreading. The edited paper is then published in its final form in a regular print and online issue of **Biol Chem.** At this time, the **Biol Chem ‘Just Accepted’ Paper** version is replaced on the journal Web site by the final version of the paper with the same DOI as the **Biol Chem ‘Just Accepted’ Paper version.**

Disclaimer

Biol Chem ‘Just Accepted’ Papers have undergone the complete peer-review process. However, none of the additional editorial preparation, which includes copy editing, typesetting and proofreading, has been performed. Therefore, there may be errors in articles published as **Biol Chem ‘Just Accepted’ Papers** that will be corrected in the final print and online version of the Journal. Any use of these articles is subject to the explicit understanding that the papers have not yet gone through the full quality control process prior to advanced publication.

Biological Chemistry **'Just Accepted' paper**
ISSN (online) 1437-4315
DOI: 10.1515/hsz-2018-0470

Research Article

CFTR structure, stability, function and regulation

Xin Meng, Jack Clews, Anca D. Cuita[a], Eleanor R. Martin and Robert C. Ford*

School of Biological Sciences, Faculty of Biology Medicine and Health, Michael Smith Building, The University of Manchester, Oxford Road, Manchester M13 9PL, UK

*Corresponding author

e-mail: bob.ford@manchester.ac.uk

[a]Current address: Institute of Molecular Biology and Biophysics, ETH Zurich, HPK G11, Otto-Stern-Weg 5, CH-8093 Zurich, Switzerland.

Abstract

CFTR (Cystic Fibrosis transmembrane conductance regulator) is a unique member of the ATP-binding cassette family of proteins because it has evolved into a channel. Mutations in CFTR cause cystic fibrosis, the most common genetic disease in people of European origins. The F508del mutation is found in about 90% of patients and here we present data that suggest its main effect is on CFTR stability rather than on the 3D folded state. A survey of recent cryo-electron microscopy studies was carried out and this highlighted differences in terms of CFTR conformation despite similarities in experimental conditions. We further studied CFTR structure under various phosphorylation states and with the CFTR-interacting protein NHERF1. The coexistence of outward-facing and inward-facing conformations under a range of experimental conditions was suggested from these data. These results are discussed in terms of structural models for channel gating, and favour the model where the mostly disordered regulatory-region of the protein acts as a channel plug.

Keywords: ABC transporter, CFTR, electron microscopy, ion channel, membrane protein structure.

Introduction: the cystic fibrosis transmembrane conductance regulator (CFTR)

CFTR is an ATP-gated chloride channel present in the apical membranes of cells lining the externally-facing surfaces of several organs (Riordan, 2008). Phosphorylation of a highly charged regulatory region (R-region) of CFTR by protein kinase A or C activates the channel, which can then open, allowing chloride ion flux, provided ATP is available (Chappe *et al.*, 2003). Chloride ions pass (passively) through the protein along their concentration gradient. Typically this means that CFTR channel opening is associated with the loss of chloride ions from the cell and their accumulation in the extracellular milieu. The charge imbalance caused by the movement of chloride is corrected by the concomitant flux of sodium ions in the same direction, and the resultant osmotic imbalance is accommodated by the flux of water into the extracellular space. Excess CFTR activity and hence water flux can lead to diarrhea (in the intestinal tract). Sub-normal CFTR activity can lead to constipation in the guts and also stasis of the mucociliary clearance mechanism, vital for maintaining healthy lungs (Donaldson *et al.*, 2006). This latter outcome is the most serious symptom for cystic fibrosis (CF) patients who have significantly reduced CFTR activity due to inheritance of two mutated and defective copies of the *cftr* gene (Riordan *et al.*, 1989). In CFTR, channel opening is associated with the outward-facing state, where the ATP-binding domains are dimerised (Cai *et al.*, 2011; Vergani *et al.*, 2005; Yeh *et al.*, 2017). CFTR channel function is also activated and controlled by phosphorylation, and here new structural data have provided different models of how phosphorylation could affect CFTR activity (Fay *et al.*, 2018; Zhang *et al.*, 2017).

Mutations in the *cftr* gene are varied, although the predominantly-observed mutation in patients of European descent is a deletion of three bases that results in the loss of a phenylalanine residue at position 508 in the protein's amino acid sequence (Riordan *et al.*, 1989; Veit *et al.*, 2016). Interestingly, deletion of this single residue (F508del) leads to a protein that is only a little worse in terms of its intrinsic channel activity (Meng *et al.*, 2017). However, it is noticeably less stable at physiological temperatures (Meng *et al.*, 2017). The unstable product is recognized and degraded by endoplasmic reticulum (ER) quality control mechanisms, and this occurs so efficiently that little or no F508del CFTR protein reaches the apical membrane (Brodsky, 2001). The high rates of occurrence of the F508del mutation (90% of patients have at least one copy) and disease (~1 in 2000 sufferers, carriage rate ~1

in 25) point to a prior selective advantage of being a carrier in humans with European origins. The exact nature of that advantage is debated (Gabriel *et al.*, 1994; Wiuf, 2001), but there is broad agreement that it is likely to be related to a strong selective pressure imposed by intestinal diseases associated with high rates of infant mortality in the past.

Biochemical and biophysical measurements of CFTR have been crucial in our understanding of the effects of the various CF-causing mutations such as F508del (Meng *et al.*, 2017; Vernon *et al.*, 2017; Yang *et al.*, 2018). Moreover, the development of fluorescence-based assays for CFTR channel activity has allowed the discovery of small molecules that can potentiate the channel activity and also rescue the instability defect (Galietta *et al.*, 2001). There are now molecules available for the treatment of most patients (Davies *et al.*, 2018; Keating *et al.*, 2018; Ren *et al.*, 2013; Yu *et al.*, 2012) (subject to cost). CFTR is somewhat unusual in that it is clearly a channel that has evolved from a group of proteins that are otherwise active transporters (Dean *et al.*, 2001). Our understanding of the CFTR protein is, to a large extent, based on prior studies with these other transporters that couple ATP hydrolysis to substrate transport across a membrane (Higgins, 1992). When compared using sequence homology and phylogenetics, CFTR has been classified into the C sub-family of the eukaryotic ATP-binding cassette transporters (Dean *et al.*, 2001). There are 38 transporter-like proteins belonging to this overall family in humans of which 13 are in the C sub-family. Two other C sub-family members are also non-transporters, and this pair have evolved as switches that control another channel (Mikhailov *et al.*, 2005). The remaining 10 members of the C sub-family are transporters and many of them are involved in xenobiotic clearance and hence associated with multi-drug resistance (Higgins, 2007; Rosenberg *et al.*, 2010).

Comparison of cryo-EM structures for CFTR

There are now several structures that have been published for CFTR. A summary of the various structures, their overall conformation and the experimental conditions employed to obtain them is proposed in Table 1.

An immediate observation based on Table I is that different conformations of the protein can be observed under very similar experimental conditions: For example the fully activated (phosphorylated) state of the protein in the presence of ATP has been reported as being in the outward-occluded conformation in two studies (Zhang *et al.*, 2017, 2018), but in another structural study, activated CFTR was found to be in the inward-facing state (Fay *et al.*, 2018).

Similarly, the absence of nucleotide was correlated with the inward-facing state in most studies (Fay *et al.*, 2018; Liu *et al.*, 2017; Zhang *et al.*, 2016), but in one study the outward-facing state was found instead (Rosenberg *et al.*, 2011). We would argue that consideration of the plasticity of ABC transporters must be taken into account. There are now several studies where a range of conformations within a population of an ABC transporter under the same conditions has been observed (Moeller *et al.*, 2015). These studies show that the separation between the NBDs can vary considerably for inward-facing conformations, and that the NBD dimerized state (outward and outward-occluded states) are sampled quite rarely, even in the presence of nucleotide and non-hydrolysable nucleotide analogues. Mutagenesis may also throw some light on these discrepancies (Table 1, column 5). Catalytic silencing of ATPase activity alone does not seem to be capable of stabilizing the outward-facing or outward-occluded states, since the H1404S mutation when combined with ATP and phosphorylation was nevertheless associated with the inward-facing state in chicken CFTR (Fay *et al.*, 2018). It seems possible, therefore, that the E1371Q mutation may favour the outward-facing state by changing the charge repulsion at the NBD-NBD interface.

CFTR channel function can be monitored at the single channel level. After activation and the addition of ATP, single CFTR channels can open and 'bursts' of current can be detected (Meng *et al.*, 2017). The bursts are punctuated by inter-burst intervals of quiescence. In activated human WT CFTR at physiological temperatures and with ATP present, the channels are closed for about 50% of the time (Meng *et al.*, 2017). Even during the bursts of current, there are rapid 'flickery' closures of extremely short duration. Rationalizing these single channel measurements using the structural data summarized in Table I is not easy and clearly all the cryo-EM structures are not determined under physiological conditions. One could propose that the outward/occluded state could represent the state of CFTR in the inter-burst duration. Alternatively, although flickery closures are transient at body temperature, low temperature may favour this state, hence the outward-occluded state could be representative of CFTR during a flickery closure.

Epitaxial 2D crystals (Rosenberg *et al.*, 2011) are unlikely to be formed by CFTR molecules with mixed conformational states, hence the crystallization process itself may select for a given conformation, perhaps explaining the observation of the outward-facing state in the absence of nucleotide. Although the phosphorylation state in the 2D crystal study could not be readily controlled, in all the other studies listed in Table I, the phosphorylation state was imposed before structural data were collected. In all the structural studies, full

phosphorylation has been associated with the disappearance of a weak sinuous density that was observed for the fully dephosphorylated state between the NBDs and intracytoplasmic loops (ICLs). This weak density was proposed to be part of the 200-residue long disordered regulatory (R) region that links the first NBD to the second TMD (Fay *et al.*, 2018; Zhang *et al.*, 2016). Hence models for how phosphorylation of the R-region regulates the channel activity could be proposed: In one model a simple steric blocking of NBD dimerization in the dephosphorylated state would prevent formation of the outward-facing state and hence channel opening (Zhang *et al.*, 2016). In the second model the dephosphorylated R-region would not only prevent dimerization but would also insert itself into the cytoplasmic entrance of the channel, blocking it like a plug (Fay *et al.*, 2018). In both these models, phosphorylation of the R-region would cause increased disorder and its dissociation from its position in the dephosphorylated state. Thus from Table 1 it would appear that a refined model for ABC transporter or CFTR conformation/function relationships is needed. We have proposed that inward-facing, outward-occluded and outward-facing states are always in equilibrium with each other and that the presence of ATP can push the balance in one direction or another (Meng *et al.*, 2018). Similarly, in CFTR, phosphorylation can influence the equilibrium, especially between the inward-facing and outward-occluded states. Whether a similar phospho-regulation mechanism exists in other ABC transporters remains to be explored.

Further regulation of the activity of CFTR

Apart from regulation via the linking R-region, CFTR activity may also be influenced via the disordered C-terminal region of the protein. In the structures listed in Table I, no density was observed for the last 40 amino acids, and indeed for the chicken CFTR studies, the C-terminal region was deliberately truncated at residue 1441 (Fay *et al.*, 2018). It is known that the CFTR C-terminus displays a PDZ-binding motif, and this allows its interaction with either of the two PDZ domains of NHERF1, a cytoplasmic soluble protein (Moyer *et al.*, 2000). NHERF1 can mediate CFTR-protein interactions with other PDZ binding motif-containing proteins via its two PDZ domains. It can also mediate interaction with the cell cytoskeleton via the Ezrin-binding domain of NHERF1 (Moyer *et al.*, 1999). This has been associated with the formation of a non-mobile pool of CFTR in epithelial cells (Haggie *et al.*, 2004; Valentine *et al.*, 2012). Links have also been proposed between CFTR-NHERF1-cytoskeleton interactions and the recycling of CFTR in the cell (Cushing *et al.*, 2008). From a structural

perspective, the details of the interaction between the NHERF1-PDZ1 domain and the last 5 residues of the CFTR C-terminal region have been well characterized (Karthikeyan *et al.*, 2001), but the overall effects of NHERF1 binding on CFTR conformation have been studied little. There is some evidence that NHERF1 binding may favour the inward-facing state of the channel (Al-Zahrani *et al.*, 2015), and it is suspected that the CFTR C-terminus may associate with the R-region when it is phosphorylated (Bozoky *et al.*, 2013). These data would point to a regulatory system where NHERF1 would bind to the dephosphorylated CFTR protein in its quiescent state.

F508 deletion

Noticeable by its absence in Table I is a structure for the F508del mutated version of CFTR. Although the effects of this mutation have been examined in the isolated NBD1 (Atwell *et al.*, 2010), only minor local changes in the conformation were noted. Furthermore these studies relied on a stabilized, more soluble NBD1 construct that may represent a 'rescued' state. Examination of the available atomic models and the maps from which they are derived suggests that the F508 residue sits at an important interface between NBD1 and TMD2. This location was predicted well before the higher resolution structures of CFTR became available (Dawson *et al.*, 2007). Surprisingly, the overall configuration of this interface remains unchanged throughout the large conformational transitions associated with channel activation (Meng *et al.*, 2018). From an engineering perspective, this implies that F508 is part of a locking-pin component rather than being part of a ball and socket joint. Hence F508 deletion may destabilize the protein by weakening the link between TMD and NBD.

In the studies described below we have tested the effects of the F508del mutation on CFTR using a biophysical and a biochemical assay. The former probes for the native folded state as well as the thermostability of the protein. The latter probes for the native folded state and can also be applied to non-purified CFTR in the membrane it was expressed in. We have also examined the effects of phosphorylation on CFTR conformations using low resolution EM and further explored the link between structure/activity and regulation with the CFTR-interacting protein NHERF1.

Results and discussion

Protein purification and characterization

The expression and purification of full-length CFTR construct with an N-terminal His-SUMOstar tag and a C-terminal GFP-His tag has been described previously (Meng *et al.*, 2017; Pollock *et al.*, 2014). WT, F508del and G551D versions of this construct were employed for the CFTR stability studies. Generation of a CFTR construct with no GFP-His tag and an authentic C-terminus was carried out for the structural studies and a purification gel is shown in Supplementary Figure 1a. The purified protein was shown to be partly phosphorylated and could be readily dephosphorylated or fully phosphorylated by treatment with the relevant enzymes (Supplementary Figure 1c,d). Full-length NHERF1, containing two PDZ binding domains and an ezrin-binding domain, was expressed in *E.coli*. A gel for the final purification step (size exclusion chromatography) is shown in Supplementary Figure 1b.

CFTR Stability: the CPM assay

We have employed a fluorescence-based assay for the stability of purified proteins that is based on the labeling of exposed Cys residues by a CPM dye (Alexandrov *et al.*, 2008; Meng *et al.*, 2017). Figure 1 summarises the data for many experiments with purified CFTR under various conditions. CFTR can be denatured thermally, whereupon more CPM will bind (to previously buried Cys residues)) giving rise to a fluorescence increase from which a mid-point unfolding temperature can be extracted (Tm). Initial labeling of exposed Cys residues at the surface of the folded protein at the start of the experiment is also a useful indicator of the native folded state, reporting on batch-to batch quality and can detect the effects of chemical denaturation (e.g. by detergent or chaotropes). For example, increasing concentrations of Guanidium HCl reduce the thermal unfolding transition temperature as well as having a major effect on the native folded state as indicated by the high initial labeling by CPM (Figure 1). Using this assay one can clearly distinguish the lower thermal stability of F508del CFTR (Figure 1a, red symbols), although there is no clear difference in terms of its initial folded state (within batch-to-batch variability). This supports earlier studies implying that F508del CFTR NBD1 was unaltered in terms of its overall 3D structure (Meng *et al.*, 2017). Acute addition of the F508del corrector drug (VX809) appears to have an effect on the initial labeling of the protein, with less exposure of Cys residues implied (square symbols), and there is a small thermostabilisation as reported before (Meng *et al.*, 2017; Meng *et al.*, 2017). In

contrast, the potentiator compound VX770 appears to have a general destabilizing effect without significantly affecting the initial labeling (triangles, Figure 1a). Interestingly, the G551D mutation, which induces the closed channel state, has a slight thermostabilising effect on the protein (blue symbols). Although the negatively charged LPG detergent has been shown to be destabilizing for isolated CFTR NBD1(Yang *et al.*, 2018) (relative to the non-ionic DDM detergent), we find that the thermostability of the G551D full-length CFTR protein is somewhat enhanced in this detergent (Figure1a, green symbols). However the CPM labeling shows an additional transition prior to the main higher temperature transition (Figure 1b). This minor transition was not included in the analysis presented in Figure 1a, but it may indicate some localised low-temperature unfolding by LPG.

CFTR stability: limited proteolysis assay

The CPM assay requires purified protein, hence it was useful to compare purified CFTR in LPG with CFTR expressed in membranes. For this we employed limited proteolysis at low temperature followed by SDS-PAGE (Figures 2 and 3). Proteolytic fragments were visualised using a C-terminal GFP tag as well as an N-terminal SUMO tag (probed with a commercial antibody). Figure 2 shows the effects of limited trypsin concentrations on C-terminal fragments generated from WT, F508del and G551D versions of the protein as described above, with the data for CFTR in microsomes on the left and for purified protein on the right. Figure 3 shows the effects of limited (25 ug/ml) and high (250ug/ml) concentrations of a different protease (thermolysin) and compares WT and F508del versions of the protein in microsomes and after purification. Both the N-terminal fragments (upper panels) and the C-terminal fragments (lower panels) are compared.

The largely unstructured R-region represents a major target for proteolytic enzymes, and hence large fragments around 100kDa, representing TMD2-NBD2-GFP and SUMO-TMD1-NBD1 can be observed at low protease levels for all CFTR variants. Lower mass C-terminal fragments can also be detected at 25 kDa (GFP) and 50-55kDa (NBD2+GFP) with both proteases, implying common protease-sensitive sites at the TMD2-NBD2 linker (55kDa fragment) and at the CFTR C-terminus (25kDa GFP fragment). Despite the presence of F508 in the N-terminal end of CFTR, no obvious differences can be detected in the N-terminal proteolytic cleavage patterns of WT and F508del CFTR (Figure 3), but the N-terminal patterns are much more complex than the equivalent C-terminal patterns. This applies to both purified CFTR as well as membrane-bound CFTR and implies that the C-terminal end of

CFTR may be susceptible to cleavage at a few, particularly sensitive, sites. Some differences in the C-terminal proteolytic cleavage patterns of F508del and WT CFTR were detected when thermolysin was employed, but not with trypsin. The formation of SDS-resistant thermolysin-GFP or thermolysin-SUMO complexes, especially at high thermolysin levels may explain these differences (Supplementary Figure 1). Overall, the conclusions from these limited proteolysis data are that F508del, G551D and WT CFTR display broadly similar sensitivity to proteases at low temperatures and that membrane-bound and detergent-purified CFTR are also similar in terms of their ability to be cleaved by soluble proteases. The discrete nature of the N-terminal and C-terminal bands with masses indicative of cleavage at major domain interfaces strongly supports the hypothesis that CFTR expressed in yeast microsomes is folded correctly and that after purification it retains a very similar overall conformation, at least at low temperatures. These data also support the hypothesis that F508 deletion mainly affects the thermostability of the protein, rather than affecting the overall fold or topology of the protein (Meng *et al.*, 2017).

CFTR structure: conformational plasticity and interaction with NHERF1

Both inward-facing and outward/occluded-facing conformations of CFTR have been reported under similar conditions (+ATP and after phosphorylation, Table I). In order to understand this dichotomy, we have proposed a model (Meng *et al.*, 2018) where CFTR can sample both conformations continuously in the presence or absence of ATP. In this model the equilibrium between inward- and outward-facing states is influenced by the presence of nucleotide and phosphorylated residues in the R-region. In order to explore this further, we studied LPG-purified CFTR single particles by negative-stain EM after phosphorylation and dephosphorylation. We also investigated whether the C-terminal interacting protein, NHERF1 had any effects on the CFTR conformational states. Figure 4a shows an example of data recorded for dephosphorylated CFTR. Single particles can be observed (circled) and these could be selected semi-automatically (Figure 4c), classified and averaged (Figure 4d). For dephosphorylated CFTR, but for none of the other conditions, short linear aggregates were also detected in these samples (Figure 4a, rectangle, Figure 4b). Similar linear aggregates were previously reported for LPG-purified CFTR where the phosphorylation status was not controlled (Al-Zahrani *et al.*, 2015), and the aggregates may be mediated by intermolecular NBD to R-region interactions which are promoted after dephosphorylation of the R-region (Bozoky *et al.*, 2013). Examination of the projection class averages for all samples implied a

mixture of inward- and outward-facing states, as expected, hence a multi-reference refinement was carried out, employing references corresponding to inward-facing and outward/occluded states that had been filtered to low resolution (40Å). Figure 4e shows the resulting 3D representations. No condition resulted in a single conformational state, indeed even dephosphorylated CFTR in the absence of ATP contained particles that gave an outward-facing structure (magenta volume) whilst phosphorylated CFTR in the presence of ATP also had a recognizably inward-facing sub-population of particles with separated NBDs (sky blue volume). Particles corresponding to the inward-facing state of dephosphorylated CFTR with NHERF1 (grey volume) had additional density between the NBDs (ellipse outline, Figure 4e and arrows, Figure 4f). It seems possible that this could represent the location of NHERF1. No other maps showed a plausible additional density close to the expected position of the C-terminal region. If correct, this would imply that NHERF1 may preferentially bind to the dephosphorylated state and may take up a discrete location in the inward-facing conformation. This concurs with earlier data showing an association of the C-terminal 40 residues with the R-region of CFTR in the phosphorylated but not dephosphorylated state (Bozoky *et al.*, 2013).

Figure 5 shows the fitting of the inward-facing human CFTR structure (PDBID 5uak) within the equivalent low-resolution map obtained from dephosphorylated CFTR. Despite the low resolution of the negative-stain structure, the overall fit is quite good, with similar separation distances between the NBDs. The LPG micelle is partly delineated and at lower density thresholds takes on the characterstic toroidal shape (shaded area and dashed red outline). Similarly the outward/occluded CFTR structural model (PDBID 6msm) fits reasonably well within the equivalent map obtained from phosphorylated CFTR in the presence of ATP. Here the detergent micelle appears somewhat smaller and less symmetric (red dashed line).

Global 3D structures representative of all particles across the various experiments were also generated (Figure 5b). These are for significantly larger datasets and show better-defined molecular outlines. The quality of the maps after global averaging suggests that CFTR is not sampling a spectrum of conformations under the varying experimental conditions employed (at least to the low resolution limits obtained here). However the inward-facing global 3D map does show some smearing of one of the NBDs, whilst the other NBD density is well defined. This could reflect some conformational flexing in the inward-facing state, but also could arise from NHERF1 binding to the CFTR C-terminal PDZ binding motif in the dephosphorylated state (Figure 4f). For the global 3D map of the outward-facing

conformation, one would expect very similar conformations as the NBDs should be tightly dimerised.

Conclusions

The studies suggest that the most common CFTR mutation (F508 deletion) mainly affects the stability of the protein rather than its overall 3D conformation. The structural studies suggest that the protein is able to sample inward-facing and outward-facing conformations in both the activated and inactivated states, and that the CFTR-interacting protein, NHERF1 may preferentially associate with the inward-facing, dephosphorylated state. The observation of the outward-facing configuration, even for the inactivated/ dephosphorylated state implies that the R-region may have a loose association between the NBDs and its steric hindrance of the NBD dimer formation observed in some structural studies is not permanent. Similarly, the presence of ATP in phosphorylated CFTR does not appear to result in a uniformly outward-facing population of molecules. Hence phosphorylation of the R-region may influence the balance between inward-facing and outward-facing conformations under physiological conditions, but does not appear to impose the outward-facing state. When comparing the various models for CFTR regulation and channel gating, the idea of the R-region acting as a phospho-regulated channel plug appears to be more consistent with the data presented here (Fay *et al.*, 2018). The plug could have a 'back-stop' function to limit unwanted leakage of chloride ions while CFTR is in the closed state rather than acting as the main channel gate. Once the plug is removed (perhaps by processive kinase activity on the multiple R-region phosphorylation sites), the unblocked protein is also free to sample conformations consistent with the open channel state.

Materials and methods

NHERF1 expression and purification

The cDNA for human NHERF1 was synthesised by Geneart Inc. and cloned into pSY5 vector (Chumnarnsilpa *et al.*, 2009) using standard ligation independent cloning methods (Aslanidis *et al.*, 1990). Plasmids were transformed into BL21 (DE3) competent *E. coli* (New England Biolabs) according to the manufacturer's instructions. Starter cultures were grown overnight at 37°C with shaking at 250 rpm in Luria broth (5 g/l yeast extract, 10 g/l peptone,

10 g/l NaCl) supplemented with 100 µg/ml ampicillin. Starter cultures were inoculated at 20 ml/l into auto-induction media (12 g/l tryptone, 24 g/l yeast extract, 9.4 g/l K_2HPO_4, 2.2 g/l KH_2PO_4, 8 ml/l glycerol 50 mM NH_4Cl, 20 mM $MgSO_4$, 5 mM Na_2SO_4, 0.3 % (w/v) α-lactose, 0.015 % (w/v) D-glucose) supplemented with 100 µg/ml ampicillin. Cultures were grown at 37°C overnight at 15°C. Cultures were harvested by centrifugation at 4200 *g*, 1 h, 4°C. Pellets were resuspended in 50 mM Tris.HCl pH 8.0, 500 mM NaCl, 20 mM imidazole and lysed using sonication then centrifuged at 19 000 *g*, 1 h, 4°C. Filtered (0.45 µm) lysates were loaded onto a 5 ml HisTrap FF Ni-NTA columns (GE healthcare) washed with the same buffer and elution was with 50 mM Tris.HCl pH 8.0, 500 mM NaCl, 250 mM imidazole. The eluted material was de-salted with 50 mM Tris.HCl pH 8.0 on a HiPrep 26/10 desalting column (GE healthcare) and loaded onto 1 mL HiTrap Q HP columns (GE healthcare). Following washing, bound NHERF1 was eluted using a gradient of 0-500 mM NaCl. Fractions were collected and further purified by size-exclusion chromatography (SEC) in 50 mM Tris.HCl pH 8.0, 150 mM NaCl using a HiLoad 16/600 Superdex 200 column (GE healthcare). Fractions were combined and concentrated using 30 kDa molecular weight cut-off concentrators and the final NHERF1 concentration was determined using the Pierce Bicinchoninic Acid (BCA) Protein Assay kit (Thermo Scientific) according to the manufacturer's instructions.

CFTR expression and purification

C-terminal eGFP* and StrepII tags were removed from opti-hCFTR within the pTR vector (Rimmington, 2014) using the Site Directed Mutatgenesis Kit (New England Biolabs) according to the manufacturer's instructions. The sequence was confirmed by DNA sequencing and transformed into competent FGY217 *S. cerevisiae* for expression and purification as previously described (O'Ryan *et al.*, 2012; Pollock *et al.*, 2014).

Phosphorylation and dephosphorylation

Purified CFTR in 50 mM Tris, pH8, 10% glycerol (v/v), 50 mM NaCl, 1 mM DTT, 0.05% LPG-14 was treated with protein kinase A (PKA) catalytic subunit (New England BioLabs, P6000) as previously described (Zhang and Chen, 2016; Liu *et al.*, 2017). PKA was diluted to 1.6 µM and incubated with CFTR at 30°C for 1 h with 0.2 mM MgATP. The dephosphorylation reaction was done in the presence of Lambda Phosphatase diluted 1:40 (w/w) at 22°C for 1 h (Lin *et al.*, 2017). Protein phosphorylation was detected with Pro-Q

Diamond stain, as described in the manufacturer's protocol (Steinberg *et al.*, 2003) and scanned using Trans-UV illumination

CFTR stability assay

The Coumarin maleimide (CPM) assay was adapted from (Alexandrov *et al.*, 2008). DTT, which interferes with the assay, was removed from the protein sample at the SEC purification step. The assay was done either in a conventional fluorimeter connected to a temperature-controlled water bath; or in an Unchained Labs UNCLE instrument using the UV laser (Meng *et al.*, 2017). For the latter, emission spectra were scanned every minute at 10°C for 30min followed by a temperature ramp to 90°C and spectra were collected at 2°C increments with a heating rate of approximately 1.5°C min^{-1}. After subtraction of buffer controls, data were analysed by integrating the tryptophan (323 nm to 350 nm) and CPM (445 nm to 463 nm) emission peaks. The ratio of the integrals CPM/Trp was employed to compensate for temperature-dependent fluorescence quenching effects and any spikes in the laser output. 1 µg purified CFTR and 0.1 µg CPM were used in each experiment.

Limited proteolysis assay

Limited proteolysis reactions were carried out at 4°C in a 20 µl reaction volume. Thermolysin (G*eobacillus stearothermophilus*) was from *Sigma* CAS # - 9073-78-3. For thermolysin, protein and microsomes were incubated with the enzyme for 15 min at 4°C and then the reaction was halted with 12mM EDTA. Purified protein was at 25µg/ml and microsomes 50 µg/ml while thermolysin was at 12.5 µg/ml or 50 µg/ml for pure protein reactions, and 25 µg/ml or 250 µg/ml for microsome reactions. The enzyme was diluted in a calcium-containing thermolysin buffer (50 mM Tris, 0.05 mM $CaCl_2$). SDS Buffer (50 mM Tris, pH7.6, 5% glycerol, 5 mM EDTA, 0.02% bromophenol blue, 4% SDS, 50mM DTT) was then added to the reaction 1:1 v:v and left at room temperature for 30 minutes before being run on a 12% polyacrylamide gel for 90 min at 130V. Limited proteolysis experiments with trypsin were conducted at 4°C for 15 minutes and stopped with a protease inhibitor cocktail (5 µg/ml E64, 48 µg/ml AEBSF, 174 µg/ml PMSF, 8.25 µg/ml Leupeptin, 8.25 µg/ml Pepstatin, 1.75 µg/ml Chymostatin, 2 µg/ml Bestatin). Protease was at a ratio of 1:75 (0.3 µg/ml trypsin) with both microsomes and purified proteins.

For Sumo identification, the gel proteins were transferred using the semi-dry method using Anode (Anode I – 30mM Tris, 20% methanol, Anode II – 300mM Tris, 20% methanol) and

Cathode (40mM 6-amino hexanoic acid, 25mM Tris, 0.01% SDS, 20% Methanol) transfer buffers. Following transfer, the membrane was incubated in 5% w/v BSA in TBST buffer (Tris Buffered Saline – 20 mM Tris (pH7.5), 150 mM NaCl, 1% Tween-20) for 1 hour at room temperature. The membrane was then incubated with an anti-Sumo primary antibody (Abcam ab176485) overnight at 4°C. Following incubation, the membrane was washed with TBST buffer 5 times for 5 min each. The membrane was incubated with a secondary antibody (Dnk pAb to Ms IgG (IRD® 800cw Abcam ab216774) for an hour at room temperature followed by 3 washes with TBST buffer for 5 minutes. The membrane was then viewed on a LiCor Odyssey machine.

Electron microscopy and structural analysis

Samples were diluted to ~25 μg/ml in 50 mM NaCl, 1 mM DTT, 0.05% LPG-14 (Mg-ATP, 2mM, was added for the phosphorylated sample) and then applied to glow-discharged EM grids and negatively-stained as described earlier (Al-Zahrani *et al.*, 2015). Image processing was carried out with the EMAN2 software package(Ludtke *et al.*, 2004). Single particles were selected using the EMAN2 interactive particle-picking tool. Classification of the projection classes allowed the removal of non-CFTR particles (discriminated by size) and aggregates (discriminated by size and shape). For most specimens this resulted in elimination of about 50% of the automatically-selected particles; about 75% were excluded for the dephosphorylated CFTR sample where linear CFTR aggregates were present. Further reclassification of the included particles identified projection classes consistent with both outward- and inward-facing CFTR particles surrounded by an annular detergent micelle. The particles were therefore further classified using the EMAN2 *multirefine* tool using two 3D reference structures (EMDB_8516 and EMDB_9230 – corresponding to inward-facing and outward-facing conformations respectively filtered to ~50Å resolution). Finally, particles classified with inward-facing or outward-facing references were separately re-refined using the single map refinement tool: Here, each dataset was split into two separately-refined subsets to allow the assessment of the resolution of the final map by Fourier shell correlation (FSC). Combination of all the particles classified with the inward-facing reference across all datasets was also carried out and this large dataset (~14 000 particles) was used for a global 3D structure refinement. A similar procedure was performed for all particles associated with the outward-facing state (~13 000 particles).

Acknowledgements

This work was partly funded by the Cystic Fibrosis Foundation (FORD13XX0) and the Cystic Fibrosis Trust (F508del CFTR SRC). EM was funded by a joint studentship between the University of Manchester and ASTAR (Singapore). We thank Prof. Robert Robinson (ASTAR Singapore); Prof. Ineke Braakman, Dr Bertrand Kleizen and Laura Tade (Utrecht) for help and insights.

Conflict of interest statement

The authors declare no conflict of interest.

References

Al-Zahrani, A., Cant, N., Kargas, V., Rimington, T., Aleksandrov, L., Riordan, J.R. and Ford, R.C. (2015). Structure of the cystic fibrosis transmembrane conductance regulator in the inward-facing conformation revealed by single particle electron microscopy. AIMS Biophys. *2*, 131-152.

Alexandrov, A.I., Mileni, M., Chien, E.Y., Hanson, M.A. and Stevens, R.C. (2008). Microscale fluorescent thermal stability assay for membrane proteins. Structure *16*, 351-359.

Aslanidis, C. and de Jong, P.J. (1990). Ligation-independent cloning of PCR products (LIC-PCR). Nucleic Acids Res. *18*, 6069-6074.

Atwell, S., Brouillette, C.G., Conners, K., Emtage, S., Gheyi, T., Guggino, W.B., Hendle, J., Hunt, J.F., Lewis, H.A., Lu, F., Protasevich, II, Rodgers, L.A., Romero, R., Wasserman, S.R., Weber, P.C., Wetmore, D., Zhang, F.F. and Zhao, X. (2010). Structures of a minimal human CFTR first nucleotide-binding domain as a monomer, head-to-tail homodimer, and pathogenic mutant. Protein Eng Des Sel. *23*, 375-384.

Bozoky, Z., Krzeminski, M., Muhandiram, R., Birtley, J.R., Al-Zahrani, A., Thomas, P.J., Frizzell, R.A., Ford, R.C. and Forman-Kay, J.D. (2013). Regulatory R region of the CFTR chloride channel is a dynamic integrator of phospho-dependent intra- and intermolecular interactions. Proc Natl Acad Sci USA *110*, E4427-E4436.

Brodsky, J.L. (2001). Chaperoning the maturation of the cystic fibrosis transmembrane conductance regulator. Am J Physiol Lung Cell Mol Physiol. *281*, L39-42.

Cai, Z., Sohma, Y., Bompadre, S.G., Sheppard, D.N. and Hwang, T.C. (2011). Application of high-resolution single-channel recording to functional studies of cystic fibrosis mutants. Methods Mol Biol. *741*, 419-441.

Chappe, V., Hinkson, D.A., Zhu, T., Chang, X.B., Riordan, J.R. and Hanrahan, J.W. (2003). Phosphorylation of protein kinase C sites in NBD1 and the R domain control CFTR channel activation by PKA. J Physiol. *548*, 39-52.

Chumnarnsilpa, S., Lee, W.L., Nag, S., Kannan, B., Larsson, M., Burtnick, L.D. and Robinson, R.C. (2009). The crystal structure of the C-terminus of adseverin reveals the actin-binding interface. Proc Natl Acad Sci USA *106*, 13719-13724.

Cushing, P.R., Fellows, A., Villone, D., Boisguerin, P. and Madden, D.R. (2008). The relative binding affinities of PDZ partners for CFTR: a biochemical basis for efficient endocytic recycling. Biochemistry *47*, 10084-10098.

Davies, J.C., Moskowitz, S.M., Brown, C., Horsley, A., Mall, M.A., McKone, E.F., Plant, B.J., Prais, D., Ramsey, B.W., Taylor-Cousar, J.L., Tullis, E., Uluer, A., McKee, C.M., Robertson, S., Shilling, R.A., Simard, C., Van Goor, F., Waltz, D., Xuan, F., Young, T., Rowe, S.M. and Group, V.X.S. (2018). VX-659-Tezacaftor-Ivacaftor in Patients with Cystic Fibrosis and One or Two Phe508del Alleles. N Engl J Med. *379*, 1599-1611.

Dawson, R.J. and Locher, K.P. (2007). Structure of the multidrug ABC transporter Sav1866 from Staphylococcus aureus in complex with AMP-PNP. FEBS Lett. *581*, 935-938.

Dean, M., Rzhetsky, A. and Allikmets, R. (2001). The human ATP-binding cassette (ABC) transporter superfamily. Genome Res. *11*, 1156-1166.

Donaldson, S.H., Bennett, W.D., Zeman, K.L., Knowles, M.R., Tarran, R. and Boucher, R.C. (2006). Mucus clearance and lung function in cystic fibrosis with hypertonic saline. N Engl J Med. *354*, 241-250.

Fay, J.F., Aleksandrov, L., Jensen, T.J., Kousouros, J.N., He, L., Aleksandrov, A.A., Gingerich, D., Riordan, J.R. and Chen, J. (2017). Cryo-Em Visualization of an Active Phosphorylated Cftr Channel. Pediatr Pulmonol. *52*, S214-S215.

Fay, J.F., Aleksandrov, L.A., Jensen, T.J., Cui, L.L., Kousouros, J.N., He, L., Aleksandrov, A.A., Gingerich, D.S., Riordan, J.R. and Chen, J.Z. (2018). Cryo-EM Visualization of an Active High Open Probability CFTR Anion Channel. Biochemistry *57*, 6234-6246.

Gabriel, S.E., Brigman, K.N., Koller, B.H., Boucher, R.C. and Stutts, M.J. (1994). Cystic fibrosis heterozygote resistance to cholera toxin in the cystic fibrosis mouse model. Science *266*, 107-109.

Galietta, L.J., Springsteel, M.F., Eda, M., Niedzinski, E.J., By, K., Haddadin, M.J., Kurth, M.J., Nantz, M.H. and Verkman, A.S. (2001). Novel CFTR chloride channel activators identified by screening of combinatorial libraries based on flavone and benzoquinolizinium lead compounds. J Biol Chem. *276*, 19723-19728.

Haggie, P.M., Stanton, B.A. and Verkman, A.S. (2004). Increased diffusional mobility of CFTR at the plasma membrane after deletion of its C-terminal PDZ binding motif. J Biol Chem. *279*, 5494-5500.

Higgins, C.F. (1992). ABC transporters: from microorganisms to man. Annu Rev Cell Biol. *8*, 67-113.

Higgins, C.F. (2007). Multiple molecular mechanisms for multidrug resistance transporters. Nature *446*, 749-757.

Karthikeyan, S., Leung, T. and Ladias, J.A. (2001). Structural basis of the Na^+/H^+ exchanger regulatory factor PDZ1 interaction with the carboxyl-terminal region of the cystic fibrosis transmembrane conductance regulator. J Biol Chem. *276*, 19683-19686.

Keating, D., Marigowda, G., Burr, L., Daines, C., Mall, M.A., McKone, E.F., Ramsey, B.W., Rowe, S.M., Sass, L.A., Tullis, E., McKee, C.M., Moskowitz, S.M., Robertson, S., Savage, J., Simard, C., Van Goor, F., Waltz, D., Xuan, F., Young, T., Taylor-Cousar, J.L. and Group, V.X.S. (2018). VX-445-Tezacaftor-Ivacaftor in Patients with Cystic Fibrosis and One or Two Phe508del Alleles. N Engl J Med. *379*, 1612-1620.

Liu, F., Zhang, Z., Csanady, L., Gadsby, D.C. and Chen, J. (2017). Molecular Structure of the Human CFTR Ion Channel. Cell *169*, 85-95 e88.

Ludtke, S.J., Chen, D.H., Song, J.L., Chuang, D.T. and Chiu, W. (2004). Seeing GroEL at 6 A resolution by single particle electron cryomicroscopy. Structure *12*, 1129-1136.

Meng, X., Clews, J., Kargas, V., Wang, X. and Ford, R.C. (2017). The cystic fibrosis transmembrane conductance regulator (CFTR) and its stability. Cell Mol Life Sci. *74*, 23-38.

Meng, X., Clews, J., Kargas, V., Wang, X.M. and Ford, R.C. (2017). The cystic fibrosis transmembrane conductance regulator (CFTR) and its stability. Cell Mol Life Sci. *74*, 23-38.

Meng, X., Clews, J., Martin, E.R., Ciuta, A.D. and Ford, R.C. (2018). The structural basis of cystic fibrosis. Biochem Soc Trans. *46*, 1093-1098.

Meng, X., Wang, Y., Wang, X., Wrennall, J.A., Rimington, T.L., Li, H., Cai, Z., Ford, R.C. and Sheppard, D.N. (2017). Two Small Molecules Restore Stability to a Subpopulation of the Cystic Fibrosis Transmembrane Conductance Regulator with the Predominant Disease-causing Mutation. J Biol Chem. *292*, 3706-3719.

Mikhailov, M.V., Campbell, J.D., de Wet, H., Shimomura, K., Zadek, B., Collins, R.F., Sansom, M.S., Ford, R.C. and Ashcroft, F.M. (2005). 3-D structural and functional characterization of the purified KATP channel complex Kir6.2-SUR1. EMBO J. *24*, 4166-4175.

Moeller, A., Lee, S.C., Tao, H., Speir, J.A., Chang, G., Urbatsch, I.L., Potter, C.S., Carragher, B. and Zhang, Q. (2015). Distinct conformational spectrum of homologous multidrug ABC transporters. Structure *23*, 450-460.

Moyer, B.D., Denton, J., Karlson, K.H., Reynolds, D., Wang, S., Mickle, J.E., Milewski, M., Cutting, G.R., Guggino, W.B., Li, M. and Stanton, B.A. (1999). A PDZ-interacting domain in CFTR is an apical membrane polarization signal. J Clin Invest. *104*, 1353-1361.

Moyer, B.D., Duhaime, M., Shaw, C., Denton, J., Reynolds, D., Karlson, K.H., Pfeiffer, J., Wang, S., Mickle, J.E., Milewski, M., Cutting, G.R., Guggino, W.B., Li, M. and Stanton, B.A. (2000). The PDZ-interacting domain of cystic fibrosis transmembrane conductance regulator is required for functional expression in the apical plasma membrane. J Biol Chem. *275*, 27069-27074.

O'Ryan, L., Rimington, T., Cant, N. and Ford, R.C. (2012). Expression and purification of the cystic fibrosis transmembrane conductance regulator protein in *Saccharomyces cerevisiae.* J Vis Exp.

Pollock, N., Cant, N., Rimington, T. and Ford, R.C. (2014). Purification of the cystic fibrosis transmembrane conductance regulator protein expressed in *Saccharomyces cerevisiae.* J Vis Exp.

Pollock, N., Cant, N., Rimington, T. and Ford, R.C. (2014). Purification of the Cystic Fibrosis Transmembrane Conductance Regulator Protein Expressed in Saccharomyces cerevisiae. J Visualized Exp.

Ren, H.Y., Grove, D.E., De La Rosa, O., Houck, S.A., Sopha, P., Van Goor, F., Hoffman, B.J. and Cyr, D.M. (2013). VX-809 corrects folding defects in cystic fibrosis transmembrane conductance regulator protein through action on membrane-spanning domain 1. Mol Biol Cell. *24*, 3016-3024.

Rimmington, T.L. (2014). Expression, Purification and Characterisation of the Cystic Fibrosis Transmembrane Conductance Regulator (CFTR) in Saccharomyces cerevisiae. In: Faculty of Life Sciences (United Kingdom: University of Manchester), pp.

Riordan, J.R. (2008). CFTR function and prospects for therapy. Annu Rev Biochem. *77*, 701-726.

Riordan, J.R., Rommens, J.M., Kerem, B., Alon, N., Rozmahel, R., Grzelczak, Z., Zielenski, J., Lok, S., Plavsic, N., Chou, J.L. and *et al.* (1989). Identification of the cystic fibrosis gene: cloning and characterization of complementary DNA. Science *245*, 1066-1073.

Rosenberg, M.F., O'Ryan, L.P., Hughes, G., Zhao, Z., Aleksandrov, L.A., Riordan, J.R. and Ford, R.C. (2011). The cystic fibrosis transmembrane conductance regulator (CFTR): three-dimensional structure and localization of a channel gate. J Biol Chem. *286*, 42647-42654.

Rosenberg, M.F., Oleschuk, C.J., Wu, P., Mao, Q., Deeley, R.G., Cole, S.P. and Ford, R.C. (2010). Structure of a human multidrug transporter in an inward-facing conformation. J Struct Biol. *170*, 540-547.

Steinberg, G.R., Rush, J.W. and Dyck, D.J. (2003). AMPK expression and phosphorylation are increased in rodent muscle after chronic leptin treatment. Am J Physiol Endocrinol Metab. *284*, E648-654.

Valentine, C.D., Lukacs, G.L., Verkman, A.S. and Haggie, P.M. (2012). Reduced PDZ interactions of rescued DeltaF508CFTR increases its cell surface mobility. J Biol Chem. *287*, 43630-43638.

Veit, G., Avramescu, R.G., Chiang, A.N., Houck, S.A., Cai, Z., Peters, K.W., Hong, J.S., Pollard, H.B., Guggino, W.B., Balch, W.E., Skach, W.R., Cutting, G.R., Frizzell, R.A., Sheppard, D.N., Cyr, D.M., Sorscher, E.J., Brodsky, J.L. and Lukacs, G.L. (2016). From CFTR biology toward combinatorial pharmacotherapy: expanded classification of cystic fibrosis mutations. Mol Biol Cell. *27*, 424-433.

Vergani, P., Lockless, S.W., Nairn, A.C. and Gadsby, D.C. (2005). CFTR channel opening by ATP-driven tight dimerization of its nucleotide-binding domains. Nature *433*, 876-880.

Vernon, R.M., Chong, P.A., Lin, H., Yang, Z., Zhou, Q., Aleksandrov, A.A., Dawson, J.E., Riordan, J.R., Brouillette, C.G., Thibodeau, P.H. and Forman-Kay, J.D. (2017). Stabilization of a nucleotide-binding domain of the cystic fibrosis transmembrane conductance regulator yields insight into disease-causing mutations. J Biol Chem. *292*, 14147-14164.

Wiuf, C. (2001). Do delta F508 heterozygotes have a selective advantage? Genet Res. *78*, 41-47.

Yang, H.B., Hou, W.T., Cheng, M.T., Jiang, Y.L., Chen, Y. and Zhou, C.Z. (2018). Structure of a MacAB-like efflux pump from *Streptococcus pneumoniae*. Nat Commun. *9*, 196.

Yang, Z., Hildebrandt, E., Jiang, F., Aleksandrov, A.A., Khazanov, N., Zhou, Q., An, J., Mezzell, A.T., Xavier, B.M., Ding, H., Riordan, J.R., Senderowitz, H., Kappes, J.C., Brouillette, C.G. and Urbatsch, I.L. (2018). Structural stability of purified human CFTR is systematically improved by mutations in nucleotide binding domain 1. Biochim Biophys Acta Biomembr. *1860*, 1193-1204.

Yeh, H.I., Sohma, Y., Conrath, K. and Hwang, T.C. (2017). A common mechanism for CFTR potentiators. J Gen Physiol. *149*, 1105-1118.

Yu, H., Burton, B., Huang, C.J., Worley, J., Cao, D., Johnson, J.P., Jr., Urrutia, A., Joubran, J., Seepersaud, S., Sussky, K., Hoffman, B.J. and Van Goor, F. (2012). Ivacaftor potentiation of multiple CFTR channels with gating mutations. J Cyst Fibros. *11*, 237-245.

Zhang, Z. and Chen, J. (2016). Atomic Structure of the Cystic Fibrosis Transmembrane Conductance Regulator. Cell *167*, 1586-1597 e1589.

Zhang, Z., Liu, F. and Chen, J. (2017). Conformational Changes of CFTR upon Phosphorylation and ATP Binding. Cell *170*, 483-491 e488.

Zhang, Z., Liu, F. and Chen, J. (2018). Molecular structure of the ATP-bound, phosphorylated human CFTR. Proc Natl Acad Sci USA

Tables and figures

Table 1 Summary of sub-nanometre resolution cryo-EM structures of full-length CFTR that have been deposited in the EMDB and PDB.

Ortholog	EMDB code	PDB code	Experimental conditions	Mutations	Overall State(s)	Ref.
Human CFTR	1966	4a82	Phosphorylation state unknown. No nucleotide. Detergent micelle. Epitaxial 2D crystals. N-linked glycosylation present.	WT with C-term His tag	OF	1
Zebrafish CFTR	8461	5uar	Dephosphorylated. No nucleotide. Detergent micelle. SPA. N-linked glycosylation.	WT	IF	2
Human CFTR	8516	5uak	Dephosphorylated. No nucleotide. Detergent micelle. SPA. N-linked glycosylation.	WT	IF	3
Zebrafish CFTR	8782	5w81	Phosphorylated. ATP present. Detergent micelle. N-linked glycosylation.	E1371Q	OO IF*	4
Chicken CFTR	7793	6d3r	Dephosphorylated. No nucleotide. Detergent micelle. SPA. N-linked glycosylation present.	Stabilising: ΔRI/H1404S/1441X C-term His tag	IF	5
Chicken CFTR	7794	6d3s	Phosphorylated. ATP present. Detergent micelle. N-linked glycosylation.	Stabilising: H1404S/ 1441X/ ΔRI/ C-term His tag	IF	5
Human CFTR	9230	6msm	Phosphorylated. ATP present. Detergent micelle. N-linked glycosylation.	E1371Q	OO	6

Key: EMDB – Electron Microscopy Databank (density map data). PDB – Protein Databank (atomic model). SPA- single particle averaging. WT – wild type sequence. OF – outward-facing state. IF – inward-facing state. OO – outward/occluded state. IF* – evidence for particles in the inward facing state co-existing with the major state. ECL – extracellular loop. C-term – C-terminal. ΔRI – deletion of residues 405–436. 1441X – truncation at this residue. References: (1) (Rosenberg *et al.*, 2012); (2) (Zhang *et al.*, 2016); (3) (Liu *et al.*, 2017); (4) (Zhang *et al.*, 2017); (5) (Fay *et al.*, 2017); (6) (Zhang *et al.*, 2018)

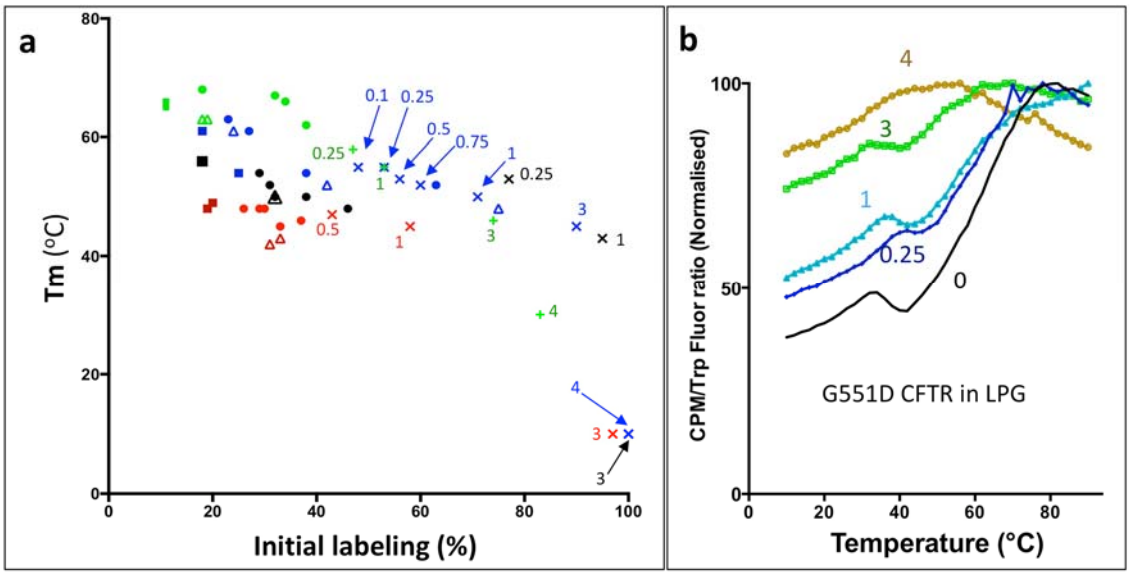

Figure 1 Thermal unfolding of CFTR.

(a) Midpoint of thermal unfolding transition (Tm) is plotted against the % of initial labeling at 10°C for several batches of CFTR and under different experimental conditions. Red, black and blue data points represent F508del, WT and G551D CFTR, respectively, purified in DDM detergent. Green points are for G551D CFTR in the presence of LPG14 detergent. Round, square and triangle symbols show the effects of no addition, VX809 (2μM) addition or VX770 (2μM) addition, respectively. Crosses and numbers show the effects of GuHCl addition, with the number indicating the final GuHCl concentration in mol/L. Where no clear thermal unfolding transition was detected (bottom right), the Tm was arbitrarily assigned to the initial labeling temperature (10°C). (b) Exemplar thermal unfolding profiles for CFTR. The data series shown are for CFTR purified in LPG and at different concentrations of GuHCl (numbers indicate molarity).

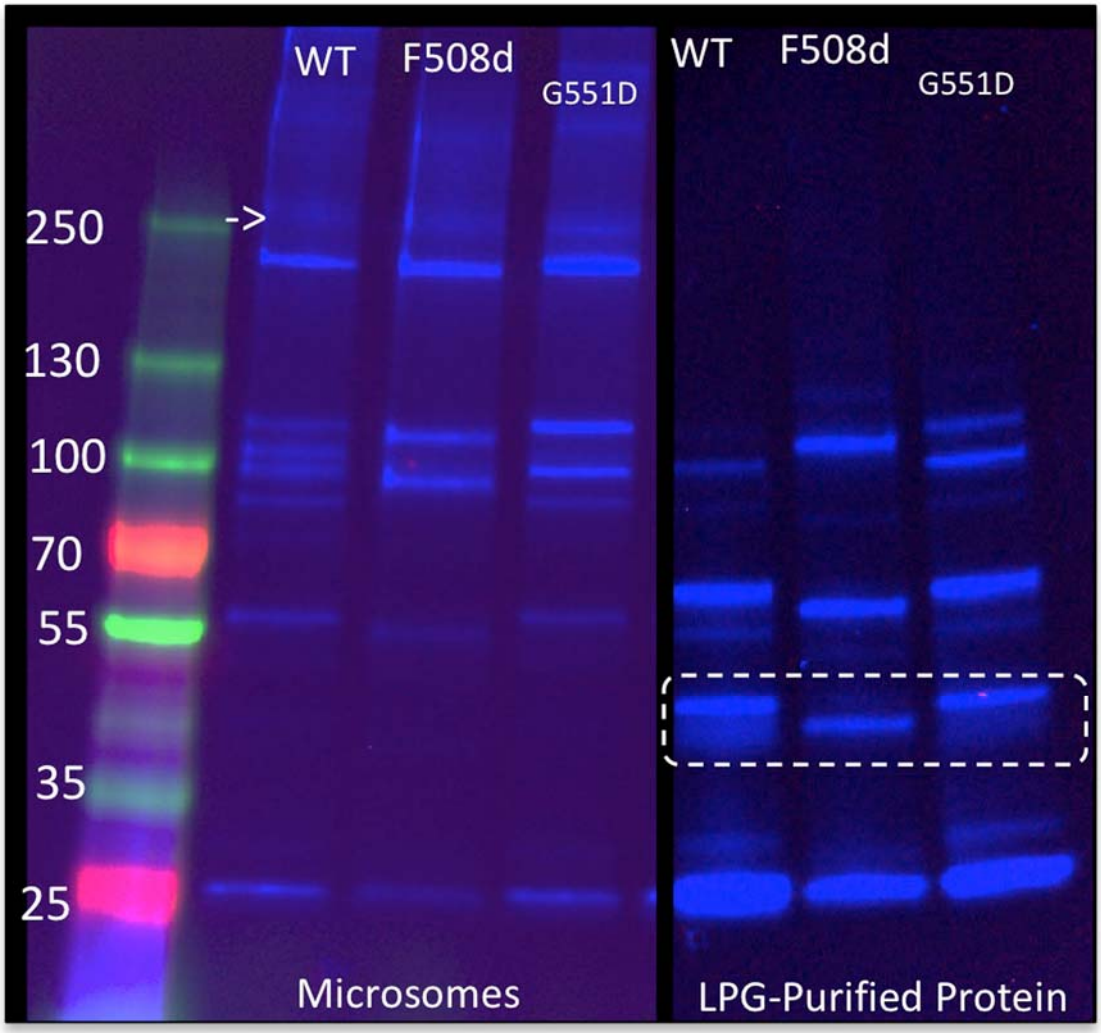

Figure 2 Limited proteolysis of CFTR variants.

Protease was at a ratio of 1:75 (0.3 μg/ml trypsin) with microsomes (left) and purified proteins (right) and detection of C-terminal fragments using the GFP fluorescence. The 25kDa lowest mass fragment is GFP alone (based on excess trypsin experiments and GFP-only controls). GFP is not unfolded by the SDS-PAGE conditions. Full-length protein runs just above the 250kDa marker and is much more protected in microsomes (arrow). The dashed rectangle outlines bands that correspond to GFP with part of NBD2, discussed in the main text.

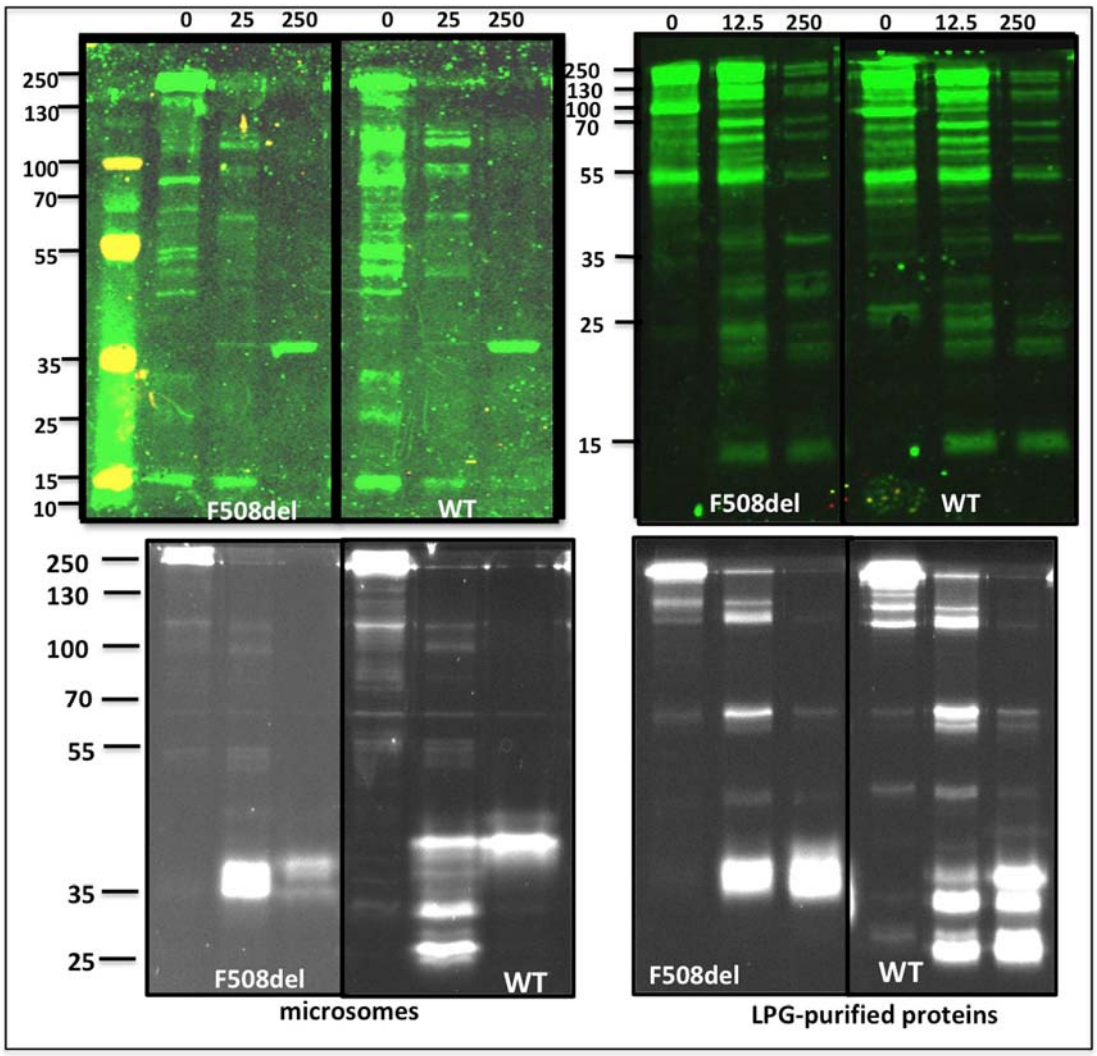

Figure 3 Limited proteolysis.

Digestion with thermolysin at a concentration of 25µg/ml and 250µg/ml with microsomes (left) or LPG-purified proteins (right). The mass ratio was 1:1 or 10:1 with microsomes and protein. The gel was probed by GFP fluorescence scan (lower panels) or subsequently Western blotted and probed with a SUMO antibody to detect the N-terminal fragments. Note that for microsomes many native yeast SUMO-ylated microsomal proteins are detected in addition to CFTR (left upper panel, no thermolysin). The overall fragmentation patterns with thermolysin are similar although some differences can be observed for the lowest mass C-terminal fragments (lower panels).

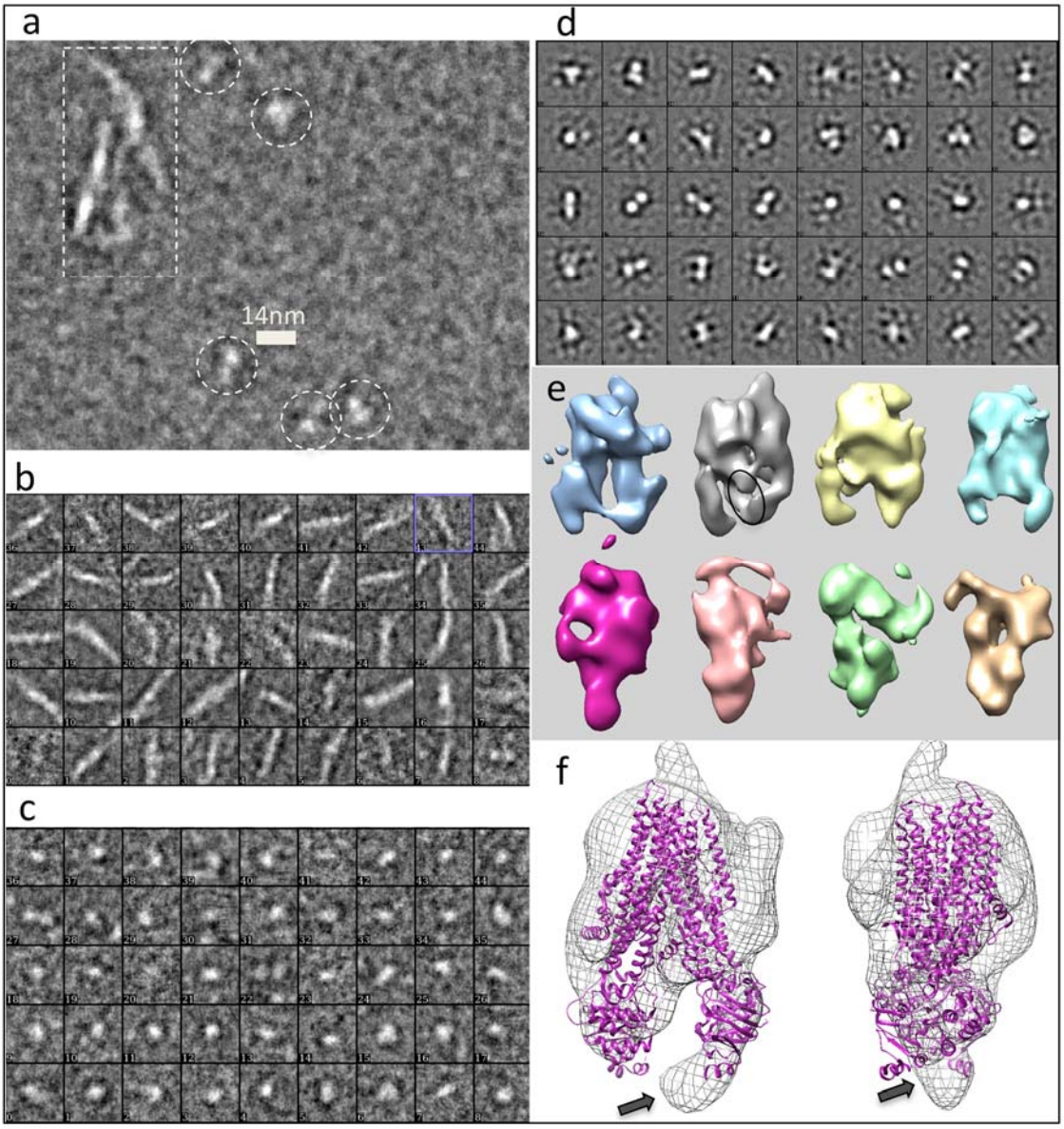

Figure 4 Electron microscopy of phosphorylated and dephosphorylated CFTR.
(a) Negatively stained micrograph of LPG-purified dephosphorylated CFTR showing 14nm diameter single particles (circled) and some linear aggregates (rectangle). (b) Examples of linear aggregates. (c) Examples of single particles. (d) 2D class averages for phosphorylated CFTR showing a mixture of inward-facing and outward-facing projection classes. Box size for panels (b-c) is 29 nm. (e) Structures of inward-facing (top) and outward-facing (bottom) 3D classes derived from (l to r): dephosphorylated CFTR; dephosphorylated CFTR + NHERF1; phosphorylated CFTR + NHERF1; phosphorylated CFTR. (f) Fitting of the dephosphorylated human CFTR structure (purple ribbon trace) to the dephosphorylated CFTR+NHERF1 map (mesh). Two orthogonal views are displayed. Additional density can be identified close to the NBD2 location after fitting (arrows).

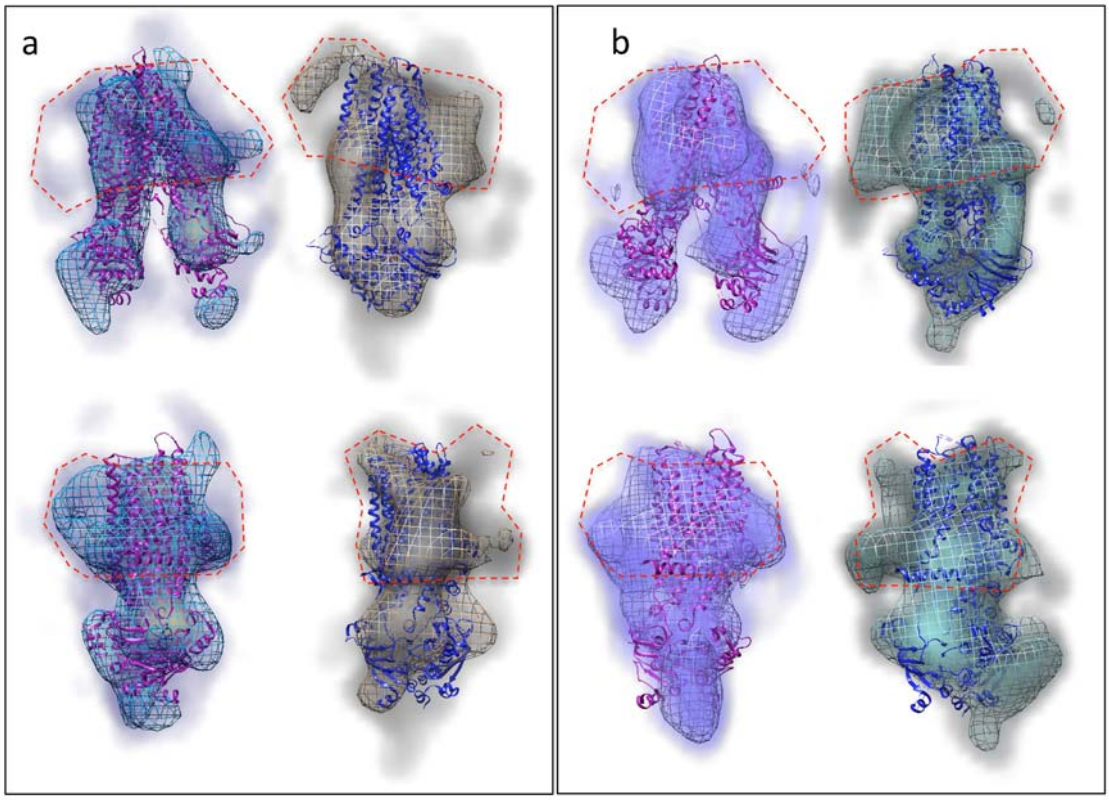

Figure 5 CFTR maps.

(a) Fitting of the inward-facing (purple, 5uak) and outward/occluded (blue, 6msm) molecular CFTR models to the equivalent low resolution maps obtained from dephosphorylated CFTR (blue mesh) and phosphorylated CFTR+ATP (brown mesh). The lower panel shows the same models/maps after rotation of each by 90^{o} around the vertical axis. At lower density threshold (shaded regions) the boundaries of the upper LPG micelle can be partially delineated (dashed red outline). (b) As in panel a, but the maps shown are global averages of all particles classified as inward-facing (left) or outward-facing (right).

Supplementary material

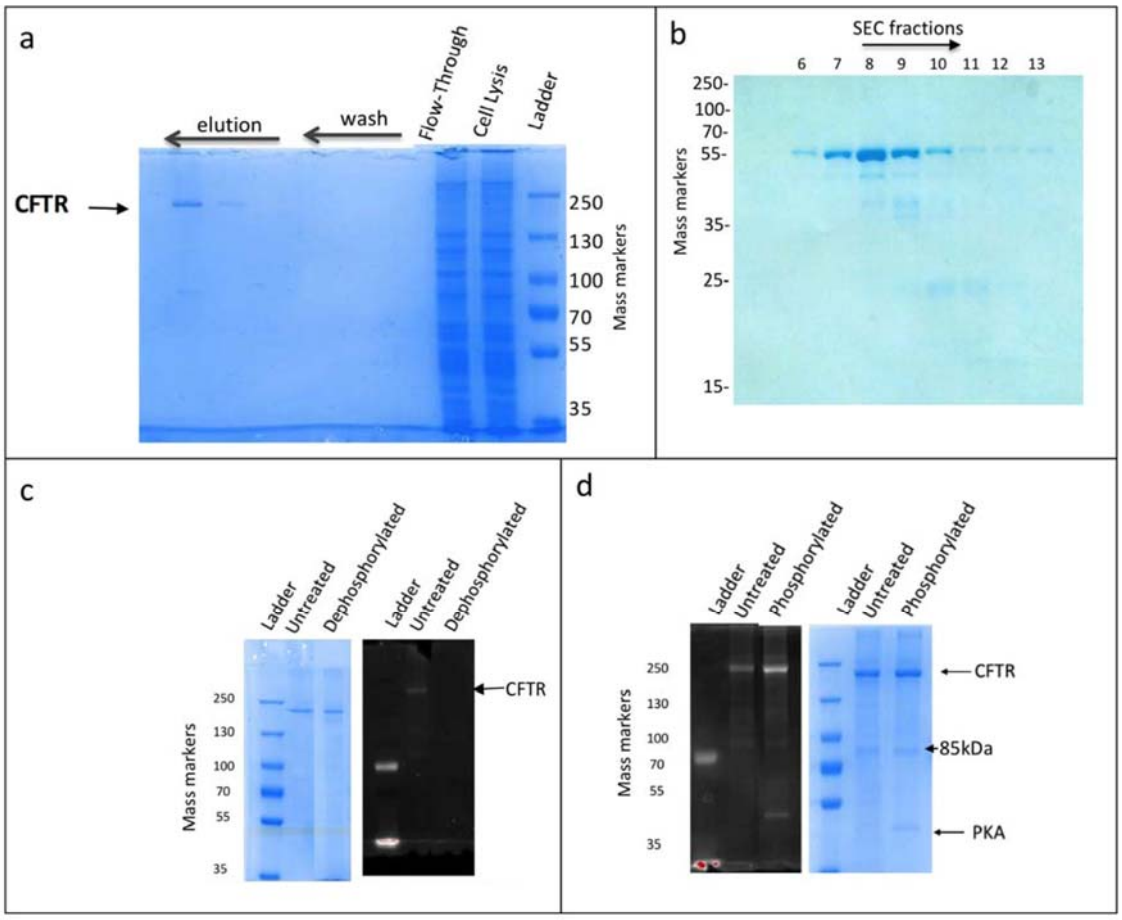

Supplementary Figure 1 Purification and characterisation of proteins:

(a) Coomassie stained SDS – PAGE purification gel for CFTR, corresponding to cell lysis extract, flow – through, wash steps and the imidazole elution fractions from the Ni – NTA purification stage, with the major CFTR band eluting at 400mM imidazole.

(b) Final purification gel for NHERF1 showing fractions from the 2nd step (size exclusion chromatography – SEC).

(c,d) LPG – purified CFTR was treated with (c) lambda phosphatase twice for 1h at 22°C or (d) PKA and 0.2mM ATP for 1h at 30°C. The blue image in each panel represents the Coomassie – stained gel with before and after treatment of CFTR samples. The greyscale image shows the Pro – Q Diamond stained SDS – PAGE counterpart, with phosphorylated protein bands showing up as white. The data shows that purified CFTR retains significant phosphorylation. A weak doublet band around 85kDa may be due to some proteolytic clipping at the R – region at 30°C which is also observed for the control untreated sample at this temperature.

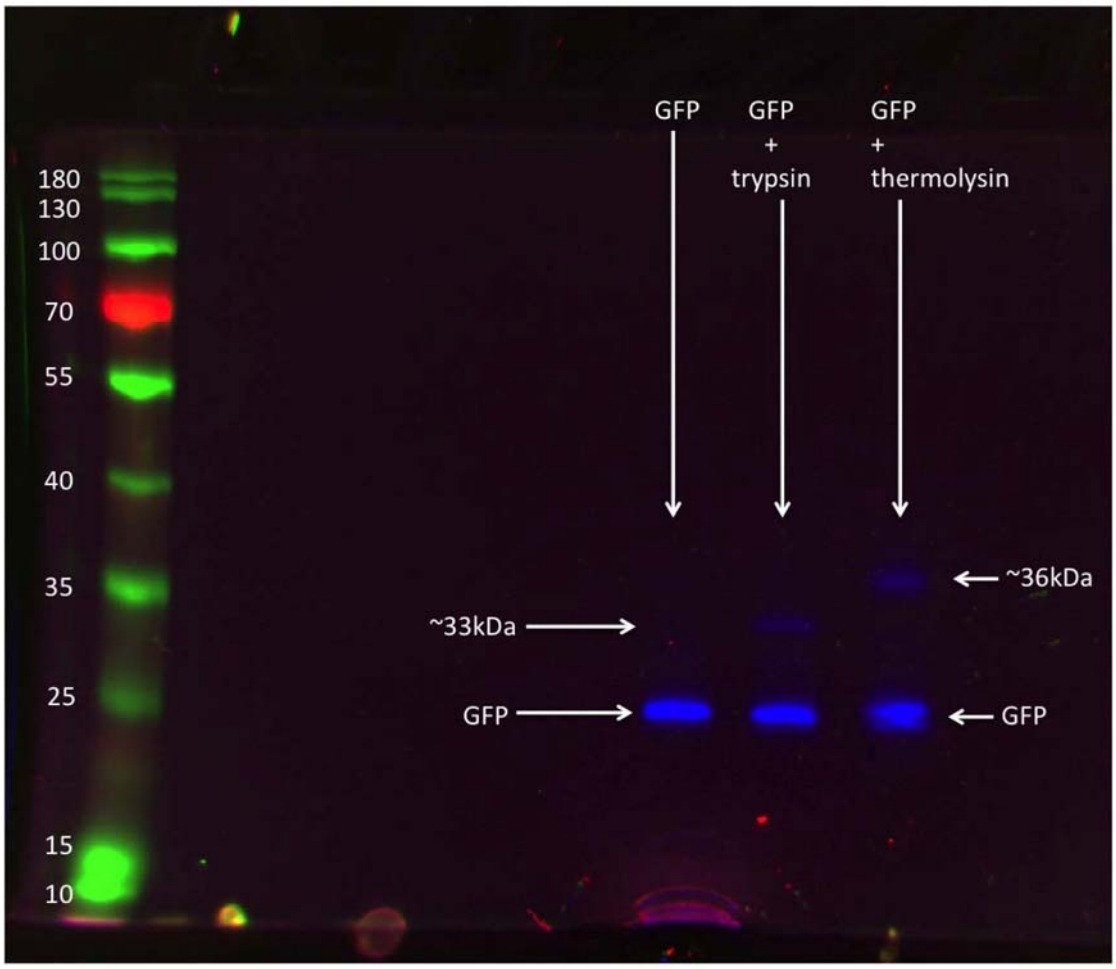

Supplementary Figure 2 GFP – only controls: GFP was treated under limited proteolysis conditions in the same way as CFTR and then run on SDS – PAGE.

GFP was resistant to degradation under the limited proteolysis conditions with both thermolysin and trypsin. Higher molecular mass fluorescent bands of ~36kDa and ~34kDa were formed in the presence of thermolysin and trypsin, respectively (indicated). A 36kDa fluorescent band was also detected after treatment of microsomes with high concentrations of thermolysin (Fig.3, main text). The formation of an SDS – stable complex between GFP and protease may be occurring.

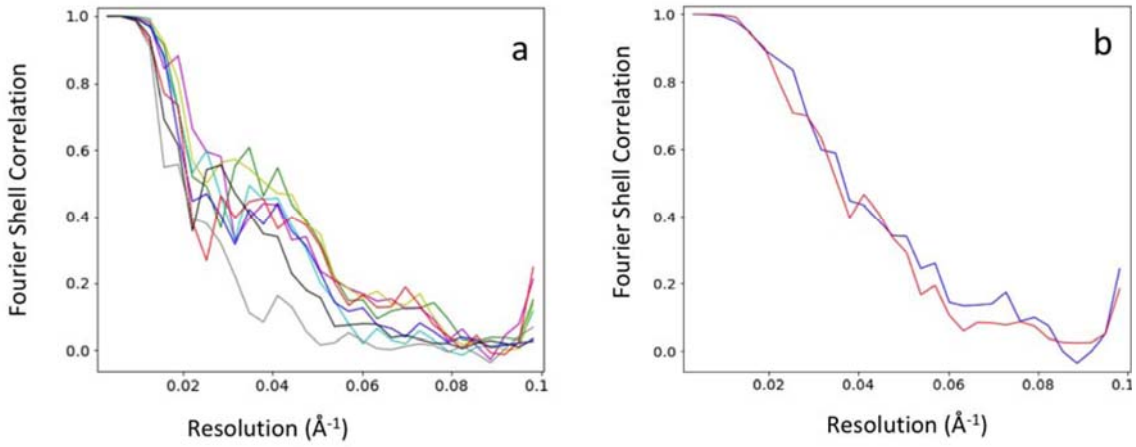

Supplementary Figure 3 Fourier shell correlation plots for CFTR 3D refinements: Black – Dephosphorylated, inward facing state. Grey – Dephosphorylated, outward facing state. Dark blue – Phosphorylated, outward facing state. Red – Phosphorylated, inward facing state. Sky blue – Dehosphorylated + NHERF1, outward facing state. Magenta – Dephosphorylated + NHERF1, inward facing state. Yellow – Phosphorylated + NHERF1, outward facing state. Green – Phosphorylated + NHERF1, inward facing state. The Dephosphorylated, outward facing state (Grey) has the lowest resolution estimate and the fewest contributing particles (635). The highest resolution at FSC=0.5, the more conservative measure, is for the Dehosphorylated + NHERF1 inward – facing dataset (Magenta) with 2719 particles. (b) Fourier – shell correlation plots for global averages of the inward – facing (blue) and outward – facing (red) states.